Multi-Body Analysis of a Tiltrotor Configuration

G. L. Ghiringhelli, P. Masarati[1] *and P. Mantegazza*
Politecnico di Milano
and
M. W. Nixon
NASA Langley Research Center

Abstract

The paper describes the aeroelastic analysis of a tiltrotor configuration. The 1/5 scale wind tunnel semispan model of the V-22 tiltrotor aircraft is considered. The analysis is performed by means of a multi-body code, based on an original formulation. The differential equilibrium problem is stated in terms of first order differential equations. The equilibrium equations of every rigid body are written, together with the definitions of the momenta. The bodies are connected by kinematic constraints, applied in form of Lagrangian multipliers. Deformable components are mainly modelled by means of beam elements, based on an original finite volume formulation. Multidisciplinar problems can be solved by adding user-defined differential equations. In the presented analysis the equations related to the control of the swash-plate of the model are considered. Advantages of a multi-body aeroelastic code over existing comprehensive rotorcraft codes include the exact modelling of the kinematics of the hub, the detailed modelling of the flexibility of critical hub components, and the possibility to simulate steady flight conditions as well as wind-up and maneuvers. The simulations described in the paper include: 1) the analysis of the aeroelastic stability, with particular regard to the proprotor/pylon instability that is peculiar to tiltrotors, 2) the determination of the dynamic behavior of the system and of the loads due to typical maneuvers, with particular regard to the conversion from helicopter to airplane mode, and 3) the stress evaluation in critical components, such as the pitch links and the conversion downstop spring.

KEYWORDS: Tiltrotor, Multi-Body Dynamics, Finite Volume Beams

Introduction

The 1/5-scale aeroelastic model of the V-22 (Figure 1) was built and tested in the period from 1983 to 1988, to support the preliminary design and the full scale development of the tiltrotor aircraft later known as the JVX. The wind tunnel tests began at the Transonic Dynamic Tunnel (TDT) of the NASA Langley Research Center (LaRC) on a semispan model, and were globally performed in three different facilities, including the Boeing Helicopter VSTOL tunnel for both the semispan and the full span model configurations. The semispan model is currently referred to as the Wing Rotor Aeroelastic Testing System (WRATS), and is located at the LaRC.

The design of a complex system as a tilting rotor aircraft requires sophisticated analyses, with different levels of approximation, as the design process matures from the preliminary, to the detailed analysis, up to the full scale development phase. Traditionally, rotors and rotor components are analysed with dedicated tools. Transfer matrix (a.k.a. Myklestad), FEA (NASTRAN, CAMRAD [11], [12], UMARC [14], DYMORE [1]) can be used for structural and modal analysis of the isolated blade; dedicated codes, based on simplified or imposed rotor kinematics, and relying on FEA for the modal characterisation of the flexibility of the rotor, can be used to find trimmed solutions of

[1]Corresponding Author,
Politecnico di Milano,
Dipartimento di Ingegneria Aerospaziale,
via La Masa 34, 20158, Milano
Tel.: ++39-2-3933-2393
Fax: ++39-2-3933-2334
E-mail: *masarati@aero.polimi.it*

the dynamics of the rotor. The family of codes that follow this philosophy is broad, and many of them have reached a high level of refinement and, expecially those developed in-house by helicopter companies, are successfully used in the design of commercial rotorcrafts (PASTA [15], DYN4-DYN5 [23]). One further step towards generality is represented by comprehensive codes, that allow a more refined modelling of the kinematics as well as of the flexibility of the system, but with some simplifications, usually represented by assuming that the rotation speed is constant and the motion is periodic, leading to the direct solution of the trim problem (CAMRAD, UMARC), an iterative solution being usually required only when a wake model is used (CAMRAD, UMARC, CAMRAD II [13]). A unifying tool, able to cover such a wide spectrum of applications, is represented by a general purpose modelling code, based on a multi-body multidisciplinary approach, that gives the analyst modelling capabilities ranging over every design step without any undue simplification. Within this framework, one can progress from rigid body models, for preliminary performance definition, to fully detailed aero-servoelastic analyses, through intermediate steps, encompassing detailed mechanism definition, introduction of deformable elements, actuators, and control system components. This approach is likely to need more computer power than that required by specialised and simplified approaches, but pays back in terms of efficiency since it allows the designer to avoid risky physical oversimplifications along with the greater modelling confidence allowed by using a single, general purpose, and well proven modelling tool. Moreover, with the computer power nowadays available, even the most complex models are likely to require a turnaround time that is compatible with an extensive set of parametric analyses and, within not so long a time, even with a complete system optimisation. Unfortunately, current commercial general purpose multi-body analysis codes, e.g. DADS [9], MECANO [3], ADAMS and others [25], still pose some limitations to the modelling of rotorcrafts, mainly due to insufficient aerodynamics, insufficient description of flexible bodies, and in some cases to limitations in the integration algorithms when applied to large finite rotations of the order of some revolutions [17].

The numerical simulations have been performed by means of an original multi-body formulation, which resulted in a code, MBDyn, that is still under development. It is intended for the simultaneous solution of multi-disciplinar problems including non-linear dynamics, aero-servoelasticity, smart piezo-structural components, electric and hydraulic components. It allows the modelling of complex systems, a clear example of which is the proposed aeroservoelastic model of a tiltrotor aircraft.

The multi-body formulation is presented first. The analytical treatment of the dynamics of rigid bodies, the handling of finite rotations, and the finite volume beam formulation are described, as well as some of the features of the multi-body code. Then the tiltrotor analytical model is described. The single components are detailed, and the steps of the build-up of the complete model are outlined. Results of intermediate analyses are presented, involving the kinematic and elastic characterisation of the hub and the modal analysis of the subparts. Finally some aeroelastic results, as well as the simulation of some typical maneuvres are presented.

Multi-Body Formulation

Dynamics. The multi-body problem is formulated by directly writing the core equations for each unknown (structural, electric, hydraulic, ...). Constraints are imposed by means of appropriate equations, with "reacting forces" as unknowns, in a way that resembles the Lagrangian Multipliers method. It should be stressed that the reaction unkowns really are the reaction forces and not abstract multipliers. This solution has been preferred to a possible generalised variational approach, to simplify the writing of the equations and thus to reduce the computational burden. Moreover, a variational formulation for non-conservative loads and constraints, and for arbitrary elements in general, like those related to the previously mentioned non-structural elements, would have been too cumbersome. For computational efficiency and simplicity of formulation, the dynamics problem has been stated as a first order differential system of equations; the equilibrium equations of a body are:

$$\begin{cases} \dot{q} - F\left(x, \dot{x}, R, \omega, \ldots, t\right) = 0 \\ \dot{\gamma} - (\omega \times S) \times \dot{x} - M\left(x, \dot{x}, R, \omega, \ldots, t\right) = 0 \end{cases}$$

where q, γ are the momenta, x is the position of the node, R is the rotation matrix that describes the rigid rotation from the local to the global frame, ω is the angular velocity of the node, that is related to the rotation matrix by the relation $\omega\times = \dot{R}R^T$[2]. The inertial forces and moments balance in a d'Alembert sense the forces F and moments M, which may depend on the configuration (i.e. on the kinematic unknowns, to give elastic forces) as well as on other parameters (like the time t). The term $(\omega \times S) \times \dot{x}$ in the moment equation is required since moments are referred to the position of the node, that is variable. The definitions of the momenta must be added, as follows:

$$\begin{cases} m\dot{x} + S \times \omega - q = 0 \\ -S \times \dot{x} + J\omega - \gamma = 0 \end{cases}$$

The mass of the body is m; the inertial properties S, J represent the first and second order inertia moments of the body and are referred to the global frame. Their transformation from the local to the global frame is given by $S = R\tilde{S}$, $J = R\tilde{J}R^T$. The physical momenta have been chosen as unknowns to let different elements with mass contribute to the inertia of a node. Kinematic constraints are added as constraint equations $\Phi\left(x, \dot{x}, R, \omega, \ldots, t\right) = 0$. The unknown constraint reactions V_F, V_M then contribute to the equilibrium equations as Lagrange multipliers. The system is summarised as follows, in a form known as Lagrangian of the first kind:

$$\begin{cases} m\dot{x} + S \times \omega - q = 0 \\ -S \times \dot{x} + J\omega - \gamma = 0 \\ \dot{q} + V_F - F\left(x, \dot{x}, R, \omega, \ldots, t\right) = 0 \\ \dot{\gamma} - (\omega \times S) \times \dot{x} + V_M - M\left(x, \dot{x}, R, \omega, \ldots, t\right) = 0 \\ \Phi\left(x, \dot{x}, R, \omega, \ldots, t\right) = 0 \end{cases}$$

The handling of the rotation matrix R is detailed in the following section and in Appendix A; it will be expressed in terms of (arbitrary) rotation parameters g. Equations Φ represent holonomic and non-holonomic constraints. In general these equations are algebraic or mixed differential-algebraic for holonomic and non-holonomic constraints respectively, and thus the system of equations is Differential Algebraic (DAE) of index three [2]. It is important to remark that the system is solved "as is", in the unknowns x, g, q, γ, V_F, V_M without any further substitution. Initial satisfaction of the constraint equations is ensured by properly assembling the joint elements in a system in which virtual springs link the nodes to their assigned positions, and then iterating until a compatible solution is obtained. This allows a great flexibility, since the initial (given) configuration may be non-compatible. Eventually the system is trimmed in a configuration that satisfies equilibrium by solving it at the initial time, with a modified update procedure that preserves the configuration and modifies only the momenta and the reaction unknowns. In this way initial equilibrium can be computed without differentiating the constraint equations up to the second order. Finally the solution is improved by iterating the so called "fictitious steps", that are normal solution steps performed at a very small time step and with high numerical damping, followed by a single-step restart of the computation. The fictitious steps implicitly perform a sort of numerical differentiation of the constraint equations without resorting to any specific procedure. General elements, called GENEL, are provided to account for user-defined generic components. They introduce user-defined unknowns a, called abstract degrees of freedom, that can interact with standard pre-existing unknowns. As a result, forces and moments may depend on abstract unknowns too, and GENEL equations are added to the system in the form:

$$\begin{cases} F, M = F, M\left(x, \dot{x}, R, \omega, a, \dot{a}, \ldots, t\right) \\ G\left(x, \dot{x}, R, \omega, a, \dot{a}, \ldots, t\right) = 0 \end{cases}$$

They are used in the preliminary development phase, to allow a high degree of flexibility in writing the formulation and the code; when a reasonable standardisation is reached, they are merged

[2]Operator $(\cdot)\times$ allows to write the vector product in matrix notation, i.e. being a a vector, $a\times$ is the matrix that multiplies vector b to give $a \times b$

in a separate family of elements. The system is being extended to the integrated simultaneous solution of multi-field problems; the active control of smart structures has been already addressed in [5] by adding electric variables and sensors, actuators and signal processing elements. Further development will involve the reinclusion of modal coordinates, and the modelling of hydraulic circuits and elements, to simulate the control system of a complete rotorcraft.

Kinematics. The formulation of the multi-body problem is based on the kinematic description of large displacements and rotations. For an accurate but efficient, i.e. fast and cheap, solution, an appropriate formulation for the rotations is fundamental. In this work, the total position of each body is used as unknown. The choice of the rotation unknowns pose a delicate problem. The orientation of a local frame is described by an orthogonal matrix R that maps vectors from the local to the global frame. The parametrisation of large rigid rotations requires at least three unknowns, but four parameters are needed to avoid singularities that arise when the orientation of the rotation is undefined. This problem has been prevented by considering incremental rotations as unknowns. So the current orientation of a reference frame R is accounted for by a constant rotation matrix R_r, that multiplies an unknown incremental rotation, held by matrix R_Δ, that is assumed to be small enough to avoid any singularity. Matrix R_r is updated after every step. A widely used three parameter parametrisation is represented by the rotational vector φ, that describes a finite rotation of amplitude given by its modulus, about an axis represented by the vector itself. A very efficient parametrisation of the finite rotations has been found in the Gibbs-Rodriguez parameters $g = 2\,\tan^{-1}(\varphi/2)$, modified with respect to the conventional notation by means of the factor 2. This makes the linearised expressions of the rotational entities concide with those of the rotational vector φ. The rotation matrix R is:

$$R = I + \frac{4}{4 + g^T g}\left(g\times + \frac{1}{2} g \times g \times\right)$$

Gibbs-Rodriguez parameters do not use trigonometric functions, that are computationally expensive. Some useful properties of the rotation matrix, and its differentiation rules, are reported in Appendix A.

Integrator. Time integration is performed by means of an implicit, A/L-stable, second order accurate, predictor-corrector integrator. The basic formulas are:

$$\begin{aligned}
\dot{y}_k &= -\frac{12}{h}\left(y_{k-1} - y_{k-2}\right) + 8\dot{y}_{k-1} + 5\dot{y}_{k-2} \\
y_k &= \left(1-\beta\right) y_{k-1} + \beta y_{k-2} \\
&\quad + h\left(\delta + \frac{1}{2}\right)\dot{y}_k + h\left(\frac{1}{2}\beta + \frac{1}{2} - 2\delta\right)\dot{y}_{k-1} + h\left(\frac{1}{2}\beta + \delta\right)\dot{y}_{k-2}
\end{aligned}$$

for the predictor, consisting in the cubic extrapolation of the derivatives based on the states and their derivatives at the two preceding steps, and the prediction of the state based on an extrapolation, the coefficients of which ensure second order accuracy, with user-defined control of the numerical damping; h is the time step. The formulas have been generalised to a variable step predictor; in this work, for sake of simplicity, only constant time step formulas are described. The coefficients β and δ can be expressed in terms of the desired asymptotic spectral radius ρ_∞, under the assumption of real and coincident asymptotic roots (best fit criterium):

$$\beta = \frac{4\rho_\infty^2 - \left(1-\rho_\infty\right)^2}{4 - \left(1-\rho_\infty\right)^2} \qquad \delta = \frac{\left(1-\rho_\infty\right)^2}{2\left(4 - \left(1-\rho_\infty\right)^2\right)}$$

For $\rho_\infty = 1$ the method is very similar to the Crank-Nicholson rule (no dissipation), though using two steps, while for $\rho_\infty = 0$ the method coincides with the well known Backward Difference Formulas (BDF) [2]. The correction is performed by means of a complete/modified Newton-Raphson iteration.

Rotations Updating. The correction is made referring to the predicted reference (this technique has been called updated-updated). The predicted frame is used as reference, so it is constant; only the rotation related to the correction is unknown. As a consequence, the unknown rotation becomes really small, provided the prediction is accurate. The angular velocity can be expressed as:

$$\omega = G_\Delta \dot{g}_\Delta + R_\Delta \omega_r$$

where subscripts $(\cdot)_\Delta$ mean that the rotation parameters and their derivatives are referred only to the correction rotation. As a consequence, when the prediction is accurate, the terms involved in the linearisations can be approximated as: $G_\Delta \cong I$, $R_\Delta \cong I$, $\Delta G_\Delta \cong 0$. The differentiations become:

$$\Delta R \cong \Delta g_\Delta \times R_r, \qquad \Delta\omega \cong \Delta\dot{g}_\Delta + \Delta g_\Delta \times \omega_r$$

this greatly simplifies the writing of the Jacobian matrix, with consequent savings in computational time. Accuracy is preserved by consistently calculating the residual. This approach can be regarded as an "intrinsically modified" Newton-Raphson solution, since the Jacobian matrix is approximated during the construction, and thus acts as a sort of very well suited preconditioner.

Constraints. Many constraints can be formulated. The most commonly used have already been implemented, to allow the modelling of common mechanisms. Table 1 lists the available elements. Most of them are based on the orthogonality condition of two vectors, namely ${e_a^i}^T e_b^j = 0$, where the subscripts refer to the bodies the vectors belong to, and the superscripts refer to the directions in the local reference frame. In Appendix B, the linearisation of basic constraints is described.

Beams. Beams represent a fundamental elastic element in the proposed multi-body implementation. The kinematic description of the generalised deformations, i.e. strains and curvatures, is based on an intrinsic formulation of the beam. The strains are defined as the difference between the current and the initial derivatives of the reference line $p(\xi)$ that describes the position of the beam. The strains, referred to the material frame, are:

$$\tilde{\varepsilon} = R_0 R^T p' - p_0'$$

where the position p refers to the current frame, while p_0 refers to the initial configuration of the beam, the prime $(\cdot)'$ performs a spatial derivative, and R_0 is the rotation matrix at point ξ in the initial configuration. The linearisation of the strains results in:

$$\Delta\tilde{\varepsilon} \cong R_0 R_r^T \left(\Delta p' + p' \times \Delta g_\Delta\right)$$

The geometric curvature $\tilde{\rho}$ is defined as the spatial derivative of the reference frame of the beam section:

$$\tilde{\rho}\times = R^T R'$$

The difference between the current and the initial, or imposed, curvature ρ_0, represents the elastic curvature $\tilde{\kappa}$, expressed in the material frame:

$$\tilde{\kappa}\times = R^T R' - R_0^T R_0' = \tilde{\rho}\times - \rho_0 \times$$

When incremental rotations are considered, the elastic curvature becomes:

$$\tilde{\kappa} = R_0 \left(R^T G g' + R_r^T \kappa_r\right)$$

After linearisation:

$$\Delta\tilde{\kappa} \cong R_0 R_r^T \Delta g_\Delta'$$

The internal forces are defined by means of a constitutive law in terms of generalised strains, i.e. $\vartheta = \vartheta(\psi)$ where ϑ are the internal forces and moments and ψ are the strains and the curvatures. An original finite volume approach is used to formulate the beam elements. A linear elastic constitutive law is usually considered, but, without any loss in generality, an arbitrary constitutive law can be considered as well, since the finite volumes formulation deals with collocated internal forces only, irrespective of their nature. Finite volumes applied to the equilibrium of a beam can be interpreted, in physical terms, as the direct balance of the forces that act on a finite piece of beam. The equilibrium equation of a finite piece of beam is:

$$(I - U_b)\,\vartheta_b - (I - U_a)\,\vartheta_a = \mathcal{F}_a^b$$

where a and b label the ends of the piece of beam, $\mathcal{F}_a^b$ are the resulting dead forces and moments applied in the interval $[a, b]$, and matrix U represents the arm of the internal forces in the equilibrium equation of the moments:

$$U(\xi) = \begin{bmatrix} 0 & 0 \\ -(p(\xi) - x)\times & 0 \end{bmatrix}$$

being x the pole the moments are referred to. A three node parabolic C^0 element has been implemented; it gives the exact solution for end-applied loads [18], [6]. The inertia of the beam is accounted for in a lumped scheme. Consistent inertia forces have been formulated, and their implementation in the linearized case showed higher accuracy in modelling the dynamics of a coarse beam model, but at a higher computational cost [6]. The finite volume beam can be regarded as a constraint that relates the reaction forces to the deformation of the link, and thus to the configuration of the system. Provided the relation between reactions and configuration is invertible (i.e. the Hessian of the strain energy is positive definite), the constraint equation can be implicitly solved, thus allowing the direct writing of the contribution of the beam to the equilibrium equations in terms of position and rotation unknowns. The loss in symmetry of the linearised matrices of the finite volumes beam is not a drawback in the context of a multi-body formulation, since the problems at hand already are non-symmetric. Finite volume beams are easy to implement in a multi-body formulation since only collocated evaluation of contributions to the equilibrium equations is required. Moreover, they straightforwardly resemble the natural partition in distinct bodies that is peculiar to the multi-body formulation. The finite volume description of the deformation of slender bodies is consistent with the mathematical, intrinsically discrete, multi-body model, and thus allows an easy but thorough modelling, especially when used in conjunction with specialised beam section analysis and characterisation formulations, like those described in [7] and [4].

Aerodynamic Forces. The aerodynamic forces are based on the strip theory, using elements that refer to rigid or beam shaped aerodynamic surfaces. The aerodynamic coefficients are based on the interpolation of experimental data spanning 360 degrees of angle of attack. Corrections are made to determine the drag due to spanwise flow, as well as the effects of dynamic stall [8]. Quasi-steady aerodynamics coefficients can be considered as an alternative approach. Rotor elements are defined, to account for the effect of rotor induced velocity with an increasing degree of refinement, from uniform up to Glauert and Mangler inflow distribution in hover and in forward flight, respectively. Dynamic inflow modelling can also be used [22]. The previous version of the code was interfaced to an aerodynamic code that models the wake of a rotor. An upgrade for the current version has been planned.

Tiltrotor Models

A tiltrotor aircraft is a complex system that has the behaviour of both a conventional airplane and of a rotorcraft, with peculiar maneuvres, e.g. the conversion. Its aerodynamics are characterised by the high influence of the rotor on the airstream that affects the wing, in both helicopter and airplane configuration. In fact the WRATS project has been mainly focused on the reduction of the vibration level induced by these interactions in the airplane mode by means of an actively controlled swashplate with the Higher Harmonic Control (HHC) technique, coupled to an active flap [20]. The blades of the rotor represent a compromise between helicopter and propeller blades. Since they are optimised for the high axial airstream speed typical of the airplane mode, they are highly twisted, thus showing high elastic couplings between twist and in- and out-of-plane bending [19]. The conversion maneuvre, when performed at typical rates for aircraft control, introduces gyroscopic effects that are unusual in conventional helicopters. The flexibility of the wing can magnify the effects of ground and air resonances, the latter being typical of automatically controlled rotorcrafts. Many of these problems are well known, but have never been faced to this extent, while others are completely new. For this reason, a particularly intensive experimental campaign preceeded and accompanied the whole development of the JVX [16], supported by numerical analyses of the related subproblems. Eigenvalue analyses of the rotor dynamics, the determination of flutter margins of the rotor, of the wing and of the ensemble, by means of analytical models based on comprehensive rotorcraft analysis codes, and dynamic simulations of the rotor mechanisms by means of early multi-body codes have been performed at each step of the wind tunnel investigations [23], [24]. Most of these analyses were performed by means of comprehensive rotorcraft codes, with properly simplified models. In this paper a different approach is proposed, consisting in the use of a single, state-of-the-art, multipurpose multi-body code that is able to perform most of the required simulations starting from a single bulk model that can be specialised for each analysis. Each subpart of the tiltrotor is modelled and analysed in its basic kinematic and dynamic features, then the parts are assembled together and the system is analysed as a whole. By using the same code and the same modelling for the single parts and the assembly, and by using a rather general approach in the kinematic and mechanical description of the single parts, any undue approximation is avoided. The tiltrotor has been split in the following subsystems:

1. The blade, made up of a flexbeam, a pitch hinge and a pitch link. Either rigid or flexible blades have been considered.

2. The gimbal, a constant velocity joint made up of its components in order to give an accurate kinematic description of the joint.

3. The swash plate, made of the two plates, the two scissors that constrain the axial rotation of the plates with respect to the pylon and to the hub, and the three non-rotating links that control the collective and the cyclic position of the plates.

4. The half-wing model, made of the deformable wing, the pylon, modelled as a rigid body, the conversion hinge, the downstop spring and the mast.

The complete model is sketched in Figure 2.

Blade. The single blade model has been used to analyse the dynamic properties of the isolated blade, such as frequencies and aerodynamic properties. Three different models have been considered, with increasing discretisation refinement. All the models share the description of the flexbeam, that uses a three-node beam element, and of the controls. The blade is joined to the flexbeam by a spherical hinge at the outer end, and by a spanwise oriented in-line joint, 2.2 in. outwards of the rotor axis. The bending of the flexbeam accounts for flexible flap and lag motion, while the pitch rotation is allowed by the bearings. A distance joint between the rotating swash-plate and an offset point aft of every blade cuff models the control link. It can be both rigid or flexible, to account for the flexibility of the control system. A rigid blade has been considered first, which proved to be poor because the yoke is very stiff, so even the very first in-plane bending mode implies appreciable deformation of the blade itself. On the other hand, the rigid blade represents an acceptable tradeoff when the performances of the rotor are addressed. A flexible blade has been subsequently modelled, with two and four beam elements respectively. The first frequencies of the cantilevered blade obtained by MBDyn are reported in Table 2, compared to Ground Vibration Tests (GVT), UMARC and NASTRAN Finite Element Analysis codes results.

Gimbal. The gimbal model has been used to determine the kinematic and gyroscopic properties of the rotor. It consists in a constant velocity joint, made by two universal joints, linked to the mast and to the hub respectively at one arm of each cross. The other arm of the crosses is connected to a linkage, that transmits the torque between the mast and the hub and keeps constant the distance between the two U-joints. The hub is also linked, by means of an in-line joint, to a spherical joint on the mast that allows the gimbal motion. The gimbal allows the rigid flapping of the whole rotor and, since the direction of the angular velocity tilts together with the hub, no Coriolis forces due to this motion result in the blades when the flapping is steady. At the same time, the 1 per rev. flapping motion has no stiffness due to centrifugal effects, but only that provided by a set of springs.

Swash Plate. The swash plate model has been used to analyse the kinematics of the control system and, together with the gimbal and the rigid blade, to evaluate the pitch-flap-lag couplings for the whole collective pitch range. It has been used also to apply the desired controls to the rotor during dynamic simulations. It consists in the two plates, modelled as rigid bodies joined by a plane hinge. The fixed plate is linked to the pylon by means of an in-line joint that forces it to translate along the mast. A fixed and a rotating scissor constrain the rotation of the two plates about the rotor axis, with respect to the pylon and the mast. Three variable distance joints are used to control its translation (collective pitch) and attitude (cyclic pitch). The elongation of the fixed control links is imposed by means of a dedicated general purpose element that splits the three fundamental control inputs, namely collective, and fore/aft and lateral cyclic pitch angles, into the elongations of the links. Figures 3–5 respectively represent the kinematic pitch-flap coupling due to the gimbal and the flexible flapping, and the control stiffness as function of the collective pitch, compared to data obtained from Bell Helicopter and model calibrations.

Wing-Pylon. The half wing model has been used for aeroelastic clearance of the isolated wing. Both dynamic and aeroelastic properties of the wing in forward flight have been analysed. It consists in two beam elements for the wing, and in the pylon, modelled with a rigid body. The pylon is connected to the wing by means of a flexible spindle, modelled with a beam element, and a downstop spring. The spindle models the conversion bearing. Its bending allows the pylon to rotate with respect to the wing about the roll and yaw axes. The conversion actuator constrains this rotation, and controls the conversion angle. In the wind tunnel model, springs with different properties are used to simulate the behavior of the conversion actuator in helicopter and airplane configuration, both on- and off-downstop. The main frequencies of the wing-pylon are reported in Table 7, compared to both GVT and NASTRAN results.

Some preliminary considerations on the flapping motion: the rotation center for the flapping due to the gimbal, namely 1 per rev. flapping, is located on the rotation axis, 2 in. above the rotor plane, while the one for the flapping due to the flexbeam deformation, namely the cone and >1 per rev. flapping, lies about 1.5 in. outboard along the blade axis. The pitch control is linked to the blade 75^o aft of the blade itself and thus introduces a pitch-flap coupling $\delta_3 \cong -15^o$ that is negative (flap up causes pitch up) for the 1 per rev. motion, and slightly positive for the flexible flapping. It is known, [10], that, for a stiff-in-plane rotor, a positive δ_3 can give raise to a pitch-flap aeroelastic instability when the first out-of-plane and in-plane frequencies nearly meet. The occurrence of this instability in the simulations required a deeper analysis of the flexibility of the yoke. In detail, the flexibility of the inner part of the yoke, from the hub to the inner pitch bearing, proved to be fundamental in describing the correct coupling between the blade pitch and the flexible, symmetric flapping motion. After this part was properly modelled, the slight, symmetric instability in the analytical model disappeared. Figure 4 shows the change in pitch-flap coupling for the cone flapping motion both for rigid and flexible root of the flexbeam.

Rotor Models. The model, consisting in the rotor with rigid/deformable blades, the gimbal and the swashplate, has been used to investigate the stability of the rotor, with particular regard to the pitch-flap-lag coupling, and to evaluate the aerodynamic response to the controls. The rigid blade model matched the out-of-plane frequencies, but gave poor results for the in-plane frequencies, so it was of little use in other than performance analyses. The flexible blade models agreed very well with available data for the low frequencies of the rotor, both in the rotating and non-rotating cases *in vacuo*. Both the single blade and the complete, three blade rotor models have been analysed. For this purpose, UMARC has been modified to allow the modelling of multiple blade rotors in the finite elements analysis module, with multiple load paths to account for the control links. Tables 3 and 4 show that the presence of the gimballed hub modifies the natural frequencies of the system by breaking the symmetry. In fact, non-symmetric modes are found, as shown both by the analysis and the experiment. Results from Bell Helicopters were available for the locked gimbal case, since they were obtained for a single blade model. They refer to an old configuration of the hub, with calibrated springs at the blade root to simulate the stiffness of the controls. These results are not completely representative of the current configuration. The GVT results with locked gimbal are also not completely significant, since the gimbal couldn't be perfectly locked. As an example, in Tables 5 and 6, the rotating frequencies of the complete, three blade rotor are reported at two typical rotating speeds and collective pitches, respectively referring to hover and cruise flight conditions.

Wing Model. The wing model shows good correlation for the lowest modes, as reported in Table 7. The results are compared to experimental measurements and to numerical results based on NASTRAN code [21]. The beam and torsion modes are strongly coupled and are influenced by the properties of the downstop, the spring that is used to lock the conversion actuator in airplane mode. At present there is no conversion actuator on the wind tunnel model, so it is simulated by a set of springs that model its stiffness in different configurations.

Wing-Rotor Models. The previously mentioned models have been merged by mounting the rotor models on the flexible wing. In the rigid blade version, the complete model has been used to evaluate the performances of the aircraft during maneuvres, an example of which is the conversion. The deformable blade model has been used to test the stability of the elastically mounted rotor and to assess the feasibility of the multi-body model for the simulation of the whole, detailed deformable system. Moreover, the effects of the flexibility of the blades on the dynamics of the system, in terms of transmission of the higher harmonics of the rotor system to the body of the aircraft, have been investigated. The first wing modes are not directly affected by the modelling of the flexibility of the rotor. The torsion mode of the wing is very close, and at some airstream speeds coincident, to the rotor speed; this gives raise to resonance that can be seen in the frequency analyses of the internal forces of the wing. Four wing modes are mainly considered: the beam, chord and torsion modes of the wing, and the so called "pylon yaw" mode, a low frequency yaw oscillation of the pylon due to the flexibility of the conversion actuator. When considered in the fixed frame, the retreating rotor modes interact with the wing modes. This can be clearly appreciated from a frequency analysis of the wing response when the rotor modes are excited. Most of these modes cannot be easily identified when the aerodynamics are modelled, since they are highly damped. For this reason, a comprehensive analysis of the structural properties of the model has been performed by simulating *in vacuo* operations, while the aeroelastic properties have been estimated in different ways. The damping of the wing modes in forward flight has been estimated by system identification of the (damped) response to a given input, as is usually done during actual wind tunnel tests, while the aeroelastic pitch-flap coupling has been estimated by measuring the phase shift between an harmonic control input and the flapping response.

Figures 6, 7 refer to a collective pitch maneuvre. They show the internal moments at the wing root and the geometric pitch of blade #1 as the collective control is raised from 0 to 10 degrees in one second. The simulation is performed in helicopter mode; the nominal hover rotation speed of 888 rpm is reached in one second to obtain a trimmed condition (not shown). There is no airstream speed. The difference between the given control and the actual pitch of the blade is due to the deformation of the flexbeam and of the flexible link.

Figures 8, 9 refer to a 5 degrees fore/aft cyclic pitch maneuvre. As the rotor tilts forwards, the high frequency in-plane modes of the wing are excited, as shown by the plot of the internal moments. The oscillations in the pitch link are 1/rev., partially due to 1/rev. flexbeam flapping that is superimposed to the gimbal flapping (which implies no appreciable pitch link loads), that is needed to counteract the gimbal springs.

Figure 10 refers to the conversion maneuvre performed by a deformable blade model. It shows the internal forces at the wing root. The conversion is performed at a 10 deg/s constant angular speed. Oscillations of the internal forces due to the untrimmed initial conditions are appreciably damped as the maneuvre proceeds to the end, at 9 s. The following abrupt raise of the internal forces is due to the transient caused by the end of the maneuvre.

The flexible blade model has been used to simulate the response to a cosinusoidal vertical gust in airplane mode, of 10 ft/s amplitude. Both the stability and the sensitivity of the tiltrotor have been addressed. Figures 11, 12 show the wing out-of-plane internal moment due to the gust at different airstream speeds, for both off- and on-downstop configurations. In figure 11 the off-downstop configuration is clearly approaching the stability boundary at 140 Kts. When the rotating speed is increased, the stability boundary moves towards lower speeds, as shown by previous analyses and experiments [23].

The deformable blade model has been used in the longest and most sophisticated performed simulations, i.e. the complete conversion. The model is made of 45 nodes, 39 rigid bodies, 31 joints of different kind, 18 beam elements, 14 aerodynamic elements for a total of 571 degrees of freedom. Initially, the rigid blade model required $\Delta t = .5 \times 10^{-3}$ s, while the deformable blade model required $\Delta t = .25 \times 10^{-3}$ s to start correctly. When a variable time step was used, during the rigid blade model simulations it grew very quickly to $3.0 \div 3.5 \times 10^{-3}$ s, while, during the deformable blade model ones, it reached about $1.0 \div 1.2 \times 10^{-3}$ s. The conversion simulation required about 4.5 hours on a Pentium PRO 200 PC for a total of 40000 fixed size time steps (10 s at $\Delta t = .25 \times 10^{-3}$ s). When performed with variable step size, it required about one hour. After the model has been refined, and a soft start has been used, the flexible blade model is able to start with $\Delta t = 10^{-3}$ s, requiring 1.1 hours on a Pentium II 333 PC.

Concluding Remarks

An original formulation for the solution of the multi-body multidisciplinary modelling of a tiltrotor has been presented. The formulation proved to be efficient without excessive simplifications. Efficiency has been enhanced while maintaining the physical meaning of both the equations and the unknowns. On the computational side, the redundancy of the formulation is exploited by a sparse solver, while the updated-updated rotation approach both reduced the computational burden and eased the writing of the jacobian matrix required by the nonlinear solver. Correctness is achieved by avoiding any undue approximation in writing the kinematic relations and by properly calculating the residuals even in presence of computationally convenient approximations of the Jacobian matrix. The use of an unconditionally stable method allows a time integration whose step is dictated essentially by the desired accuracy. A model of the tiltrotor used in WRATS investigation has been analysed, consisting in rotor models of increasing refinement, with rigid and flexible blades, the gimballed constant velocity joint, the swashplate and the control links, the pylon, the conversion hinge and the flexible wing. Aerodynamic loads have been considered, to simulate different test conditions, from aeroelastic stability investigations to the simulation of complex manoeuvers, including conversion and blade pitch control. The adopted approach represents an interesting way to perform analyses of complex systems, of which the tiltrotor model is a clear example, and can lead to a valid and thorough design tool. It is worth underlining that the results here presented are meant to assess the validity of the formulation and of the code, rather than a complete analysis of the WRATS tiltrotor model. The simulations have been performed on a Pentium Pro 200 and on a Pentium II 333 PCs using Linux OS. In view of the proof-of-concept code perspective, the basic problem solving engine is retained to be significant a competitor with respect to corresponding state-of-the-art commercial codes, but it lacks in the pre- and post-processing features of such softwares. Since, even if substantially sound and robust, Linux compilers are not as effective as proprietary compilers used on the most powerful available RISC workstations, it is expected that significantly better performances can be obtained in a real industrial design environment even with the code "as is". Nonetheless enhancements are planned for the adaptive time step control in the integration, for more effective iterative solvers and for a rough low cost coarse scale parallel implementation on PCs using message passing paradigms.

Aknowledgments

The authors wish to aknowledge the NASA Langley Research Center and the ARL, which cooperated in providing data for the correlation studies.

References

[1] Bauchau, O. A., and N. K. Kang, "A Multibody Formulation for Helicopter Structural Dynamic Analysis", *Journal of the American Helicopter Society*, Vol. 38, N. 2, April 1986, pp. 3–14

[2] Brenan, K. E., S. L. Campbell and L. R. Petzold, "*Numerical Solution of Initial-Value Problems in Differential-Algebraic Equations*", North-Holland, New York, 1989

[3] Cardona A., "An Integrated Approach to Mechanism Analysis" Thèse de doctorat, Université de Liège, 1989

[4] Ghiringhelli, G. L. and P. Mantegazza, 1994, "Linear, Straight and Untwisted Anisotropic Beam Section Properties From Solid Finite Elements", *Composites Engineering* Vol. 4, N. 12

[5] Ghiringhelli, G. L., P. Masarati and P. Mantegazza, "Multi-Body Aeroelastic Analysis of Smart Rotor Blades, Actuated by Means of Piezo-Electric Devices", *CEAS Int. Forum on Aeroelasticity and Structural Dynamics*, June 17–20 1997, Rome, Italy

[6] Ghiringhelli, G. L., P. Masarati and P. Mantegazza, "A Multi-Body Implementation of Finite Volume Beams", accepted for publication in the *AIAA Journal*

[7] Giavotto, V., M. Borri, P. Mantegazza, G.L. Ghiringhelli, V. Caramaschi, G.C. Maffioli and F. Mussi, 1983, "Anisotropic Beam Theory and Applications", *Computer & Structures*, Vol. 16, No. 1–4

[8] Harris, F. D., Tarzanin, F. J. Jr., and Fisher, R. K. Jr., "Rotor High Speed Performance, Theory vs. Test", *Journal of the American Helicopter Society*, Vol. 15, No. 3, July, 1970, pp. 35–41

[9] Haug, E. J., *Computer Aided Kinematics and Dynamics of Mechanical Systems. Vol. 1: Basic Methods* Boston, Allyn and Bacon, 1989

[10] Johnson, W., *Helicopter Theory*, Princeton University Press, 1980, Princeton, New Jersey

[11] Johnson, W., "Development of a Comprehensive Analysis for Rotorcraft — I. Rotor Model and Wake Analysis", *Vertica*, Vol. 5, 1981, pp. 99–129

[12] Johnson, W., "Development of a Comprehensive Analysis for Rotorcraft — II. Aircraft Model, Solution Procedure and Applications", *Vertica*, Vol. 5, 1981, pp. 185–216

[13] Johnson, W., "Technology Drivers in the Development of CAMRAD II", presented at the *American Helicopter Society Aeromechanics Specialists Conference*, San Francisco, California, January 19–21, 1994

[14] Hong, C. H., and Chopra, I., "Aeroelastic Stability Analysis of a Composite Rotor Blade", *Journal of the American Helicopter Society*, Vol. 30, No. 2, 1985, pp. 57–67

[15] Kvaternik, R. G., "Studies in Tilt-Rotor VTOL Aircraft Aeroelasticity", Ph.D. Thesis, Case Western Reserve Univ., 1973

[16] Kwaternik, R. G., "A Review of Some Tilt-Rotor Aeroelastic Research at NASA-Langley", *J. of Aircraft*, Vol. 13, No. 5, May, 1976, pp. 357–363

[17] Lanz, M., P. Mantegazza and P. Faure Ragani, "Aeroelastic Rotor Dynamics by General Finite Element and Multibody Approaches", *IX World Congress on the Theory of Machines and Mechanisms*, Vol. 2, pp. 1650–1656, August-September 1995, Milano, Italy

[18] Masarati, P. and P. Mantegazza, "On the C^0 Discretisation of Beams by Finite Elements and Finite Volumes", *l'Aerotecnica Missili e Spazio*, Vol. 75, pp. 77–86, 1997

[19] Nixon, M. W., "Aeroelastic Response and Stability of Tiltrotors with Elastically-Coupled Composite Rotor Blades", Ph.D. Thesis, University of Maryland, 1993

[20] Nixon, M. W., Kwaternik, R. G., Settle, T. B., "Higher Harmonic Control Tiltrotor Vibration Reduction", *CEAS Int. Forum on Aeroelasticity and Structural Dynamics*, June 17–20 1997, Rome, Italy

[21] Parham, T. Jr., "A3B Semispan Model Stress Report", Bell Helicopter Internal Report No. 599-099-197, Nov. 11, 1994

[22] Pitt, M., and Peters, D. A., "Theoretical Prediction of Dynamic-Inflow Derivatives", *Vertica*, Vol. 5, 1981

[23] Popelka, D., M. Sheffler, J. Bilger, "Correlation of Test and Analysis for the 1/5-Scale V-22 Aeroelastic Model" *Journal of the American Helicopter Society*, Vol. 32, (2), Apr. 1987

[24] Settle, T. B., and D. L. Kidd, "Evolution and Test History of the V-22 0.2-Scale Aeroelastic Model", *Journal of the American Helicopter Society*, Vol. 37, (1), Jan. 1992

[25] Schiehlen, W., "Multibody Systems Handbook", Berlin Springer-Verlag, 1990

Appendix A: Finite Rotations

The differentiation of a vector $v = R\tilde{v}$ that is constant in a local frame is:

$$v' = R'\tilde{v} = R'R^T v$$

where the orthogonality of matrix R has been exploited, that is, the scalar product of two vectors does not depend on the reference frame: $a^T b \equiv \tilde{a}^T \tilde{b}$, from which follows that $R^T R = I$. When total Gibbs-Rodriguez rotation parameters g are used, the following expression holds:

$$R'R^T = (Gg') \times$$

with matrix G given by:

$$G = \frac{4}{4 + g^T g} \left(I + \frac{1}{2} g \times \right)$$

Since matrix G depends on the rotation parameters only, the derivative of matrix R linearly depends on the derivatives of the rotation parameters. When differentiating with respect to time, or linearizing, $\dot{g}$ or Δg must be respectively used instead of g'. Then the differentiation of matrix R assumes the meaning of angular velocity $\omega = G\dot{g}$ and of rotation perturbation $\theta_\Delta = (G\Delta g)$ respectively. It is apparent that if parameters g are assumed to be small, matrix G can be approximated with an identity matrix I, in the spirit of the updated-updated rotation approach.

Appendix B: Simple Constraints

As an example, two basic constraints are outlined. Most of the constraints can be obtained as a combination of the coincidence and orthogonality conditions here presented.

1. **Coincidence.** Let x_i and p_i, $i = 1, 2$, represent the position of two independent nodes $1, 2$ and the offset from the nodes to the position of the joint, both in the global frame. For sake of simplicity, the offsets p_i are assumed to be constant in the local frame. The constraint equation is:

   $$(x_2 + p_2) - (x_1 + p_1) = 0$$

   This constraint generates a reacting force f at the coincidence point, which on turn results in a force at the two nodes, and a couple due to the offsets:

   $$F = \pm f \qquad\qquad M = \pm p_i \times f$$

   The differentiation of the constraint and of the reactions gives:

   $$(\Delta x_2 - p_2 \times \theta_{\Delta 2}) - (\Delta x_1 - p_1 \times \theta_{\Delta 1}) = -(x_2 + p_2) + (x_1 + p_1)$$

   $$\pm \Delta f = \mp f \qquad\qquad \pm (p_i \times \Delta f - f \times p_i \times \theta_{\Delta i}) = \mp p_i \times f$$

   where θ_Δ refers to the perturbation of rotation, namely $G\Delta g$.

2. **Orthogonality.** Let e_i, $i = 1, 2$, represent the unit vectors of some coordinate direction referred to two independent nodes $1, 2$ and expressed in the global frame. The orthogonality constraint equation is:

   $$e_2^T e_1 = 0$$

   This constraint generates a reacting couple m that is scalar, and acts in direction $e_2 \times e_1$:

   $$M = \pm (e_2 \times e_1) m$$

   The differentiation gives:

   $$(e_2 \times e_1)^T \theta_{\Delta 2} - (e_2 \times e_1)^T \theta_{\Delta 1} = -e_2^T e_1$$

   $$\pm m (e_1 \times e_2 \times \theta_{\Delta 2} - e_2 \times e_1 \times \theta_{\Delta 1}) \pm (e_2 \times e_1) \Delta m = \mp (e_2 \times e_1) m$$

   By adding 1, 2 and 3 constraints of this kind, universal, plane and prismatic hinges can be respectively obtained.

Table 1: *List of available elements*

Aerodynamic	Rigid
	Beam
	Induced Velocity - Rotor
Dynamic Constraints	Beam
	Rod
	Spring
	Hinge
External	Force
	Couple
General	Generic Sensors Dynamics
	Swash Plate Controls
	Discrete Time Linear Control
	User Defined Element
Inertia	Lumped Mass
Kinematic Constraints	Clamp
	Distance
	Spherical Hinge
	Universal Hinge
	Plane Hinge
	In-Plane
	Prismatic
	Imposed Velocity
	Imposed Angular Velocity

Table 2: *Cantilevered blade frequencies, Hz*

Mode	Exp	UMARC	NASTRAN	MBDyn	
				4 elem.	2 elem.
1 Beam	12.29	12.3	11.5	11.3	11.7
1 Chord	34.11	34.1	33.4	33.1	32.7
2 Beam	52.44	53.0	56.7	55.8	55.0
1 Tors.	113.35	111.4	127.0	119.0	122.0

Table 3: *Single blade with flexbeam (locked gimbal), non-rotating, Hz*

Mode	BELL		GVT	UMARC	MBDyn	
	10 deg.	50 deg.	10 deg.	10 deg.	10 deg.	50 deg.
Cone	6.6	7.2	6.6	6.3	6.8	7.8
2 F	26.6	35.1	25.2	30.8	28.5	39.0
3 F	68.8	77.3	69.3	77.9	73.5	82.0
1 L	19.3	12.5	20.6	19.3	19.5	12.6
1 T	114.5	109.9	112.6	110.0	109.0	107.0

Table 4: *Full rotor (free gimbal), non-rotating, Hz*

Mode	GVT	MBDyn	
	10 deg.	10 deg.	50 deg.
Gimbal	2.0	1.8	1.5
Cone	6.8	7.0	7.8
2 Flap	25.0	26.5	36.5
2 Flap asym.	64.2	57.1	55.0
3 Flap	76.2	78.0	82.5
1 Lag	19.7	19.0	12.7
2 Lag	91.3	98.0	92.0
1 Torsion	112.1	109.0	107.5

Table 5: *Rotating frequencies, 888 rpm,* $\theta_{75\%} = -3$ *deg, Hz*

Mode	Myklestad	UMARC	MBDyn
Gimbal	-	14.8	14.8
Cone	17.2	17.3	17.5
1 Lag	22.4	20.8	24.0
Coll Lag	42.	44.0	36.0
2 Flap	37.33	49.6	41.0
2 Flap asym.	-	70.2	65.0
3 Flap	75.33	90.3	73.0
Flap/Torsion	89.33	92.7	90.0
Lag/Torsion	-	113.4	104.0
Torsion	-	116.0	110.0

Table 6: *Rotating frequencies, 742 rpm,* $\theta_{75\%} = 55$ *deg, Hz*

Mode	Myklestad	UMARC	MBDyn
Gimbal	-	12.4	12.6
Cone	14.7	14.9	15.1
1 Lag	15.3	15.8	16.5
2 Flap asym.	-	42.3	44.2
Coll Lag	32.7	45.9	46.9
2 Flap	45.3	45.6	49.1
3 Flap asym.	-	46.9	60.3
3 Flap	66.0	60.1	65.2
Flap/Torsion	89.3	90.6	97.8
Lag/Torsion	90.0	90.8	89.7
3 Lag	-	92.0	92.9
Torsion	-	116.0	108.5

Table 7: *Wing frequencies, Hz*

Mode	downstop	GVT	NASTRAN	MBDyn
Beam	on	6.00	6.16	5.9
	off	5.51	5.45	5.4
Chord	on	8.45	9.33	9.1
	off	8.45	8.74	8.8
Torsion	on	12.5	12.6	12.5
	off	10.6	10.6	11.0
Pylon Yaw	on	16.5	18.9	17.2
	off	16.7	16.7	16.6

Figure 1: *WRATS Model at Langley's TDT*

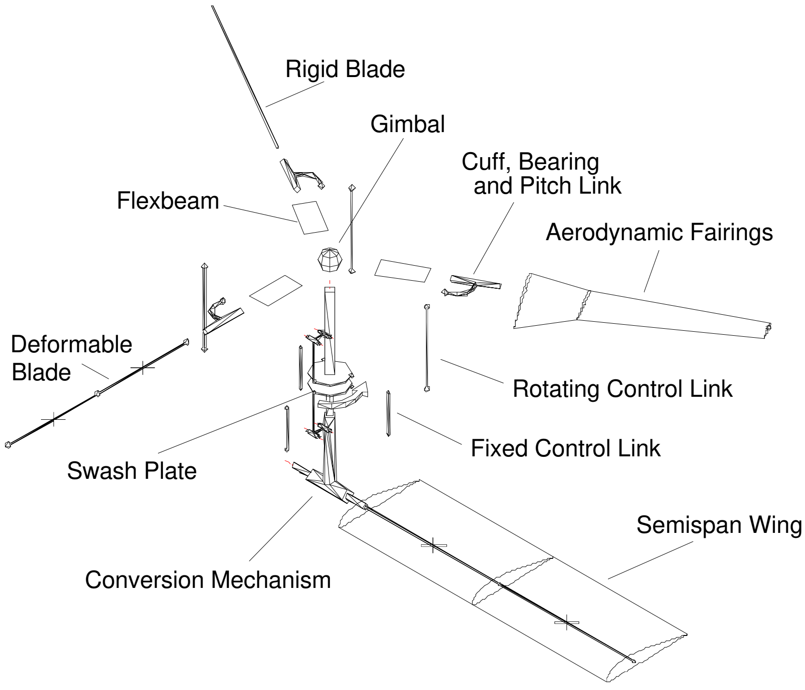

Figure 2: *Analytical Model*

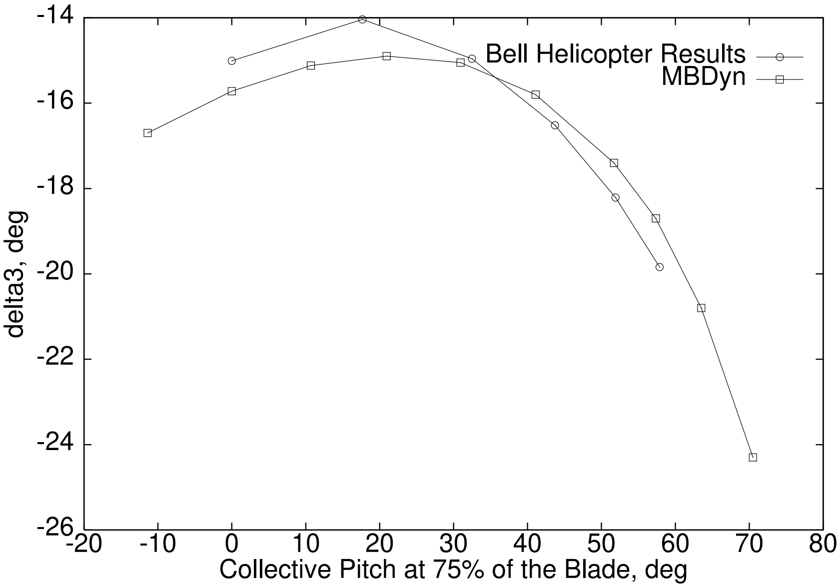

Figure 3: *Pitch-flap coupling as function of the collective pitch* $\theta_{75\%}$

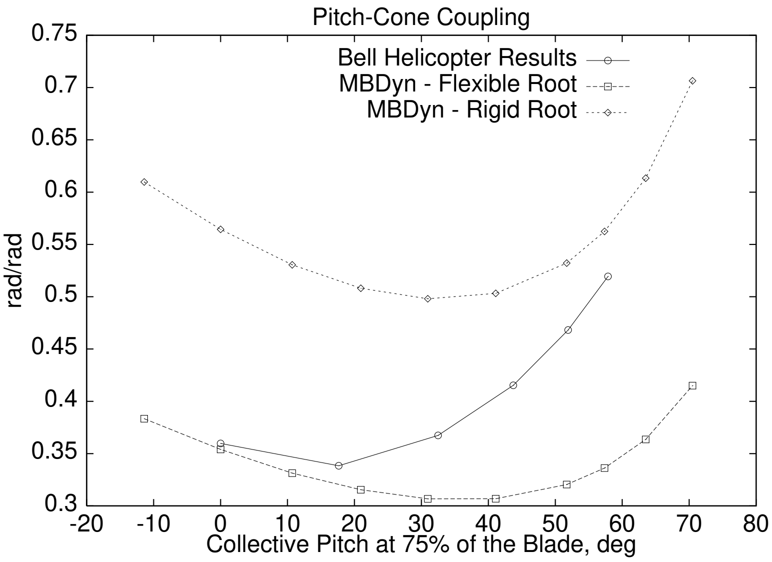

Figure 4: *Pitch-cone coupling as function of the collective pitch* $\theta_{75\%}$

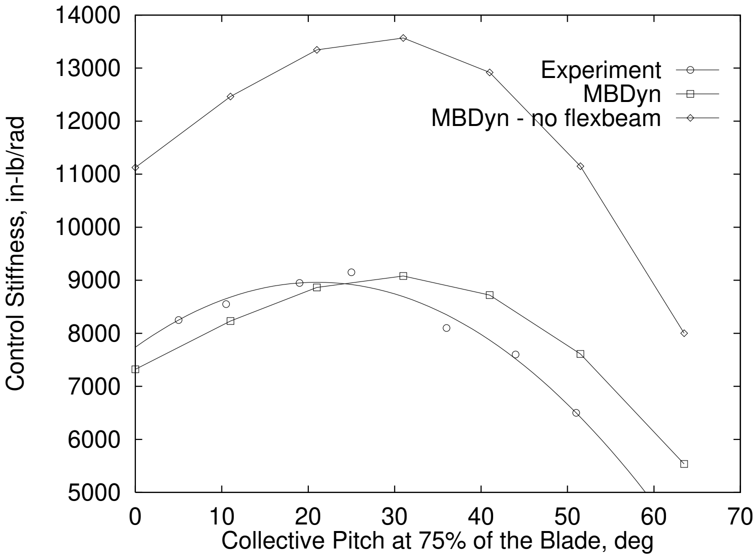

Figure 5: *Control stiffness as function of the collective pitch* $\theta_{75\%}$

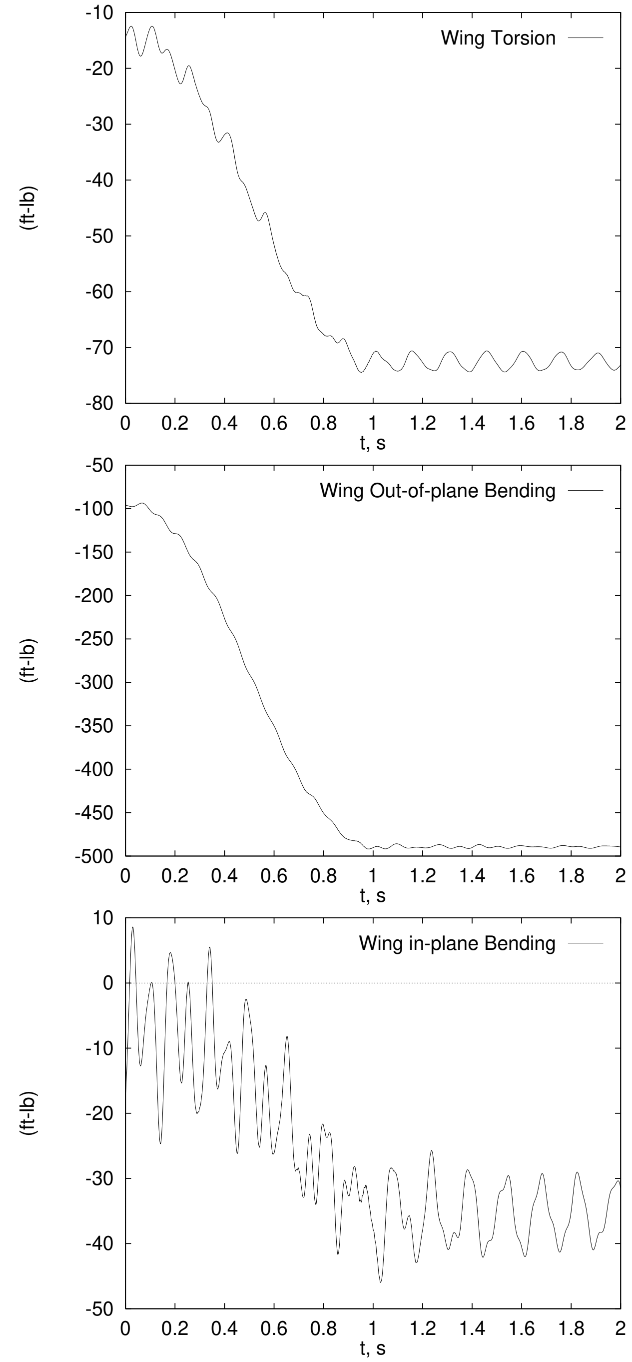

Figure 6: *Internal moments at the wing root during a 10^o collective pitch maneuvre, flexible blade model*

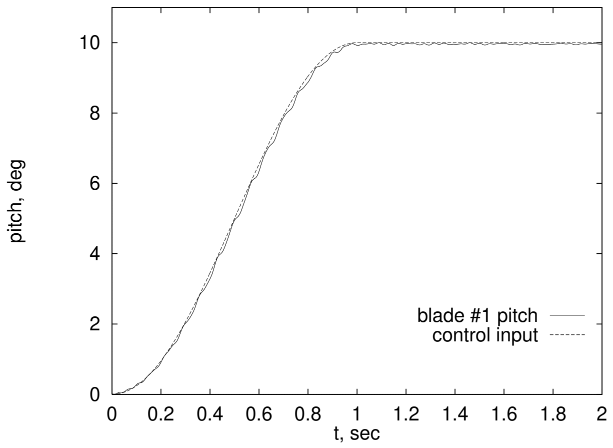

Figure 7: *Blade #1 pitch during a 10^O collective pitch maneuvre, flexible blade model*

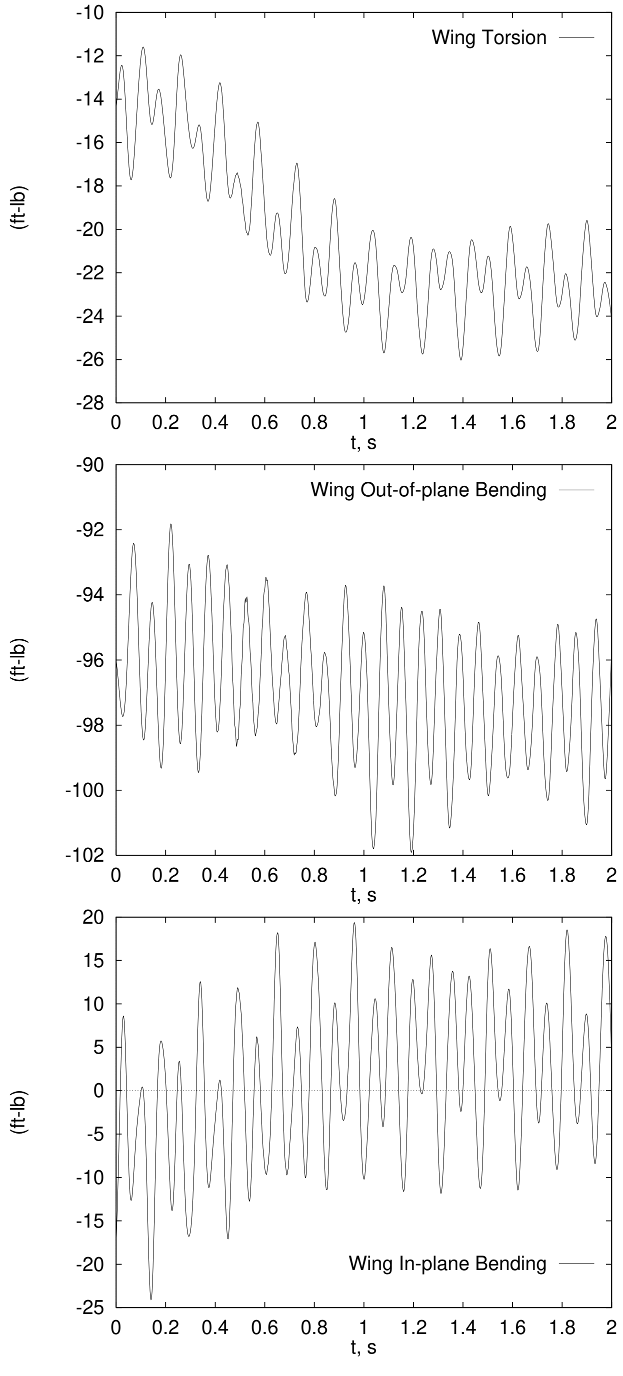

Figure 8: *Internal moments at the wing root during a 5^o fore/aft cyclic pitch maneuvre, flexible blade model*

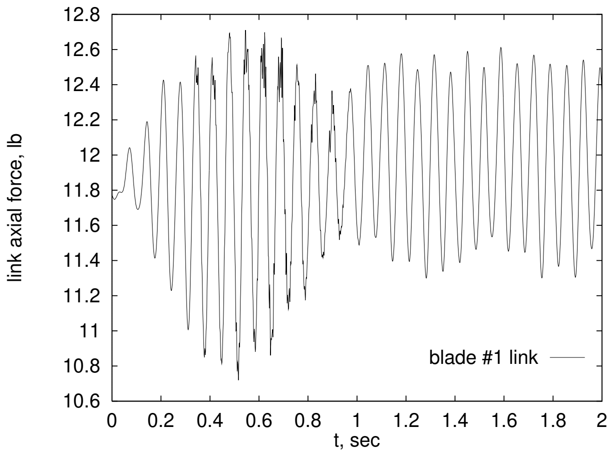

Figure 9: *Blade #1 control link axial force during a 5^o fore/aft cyclic pitch maneuvre, flexible blade model*

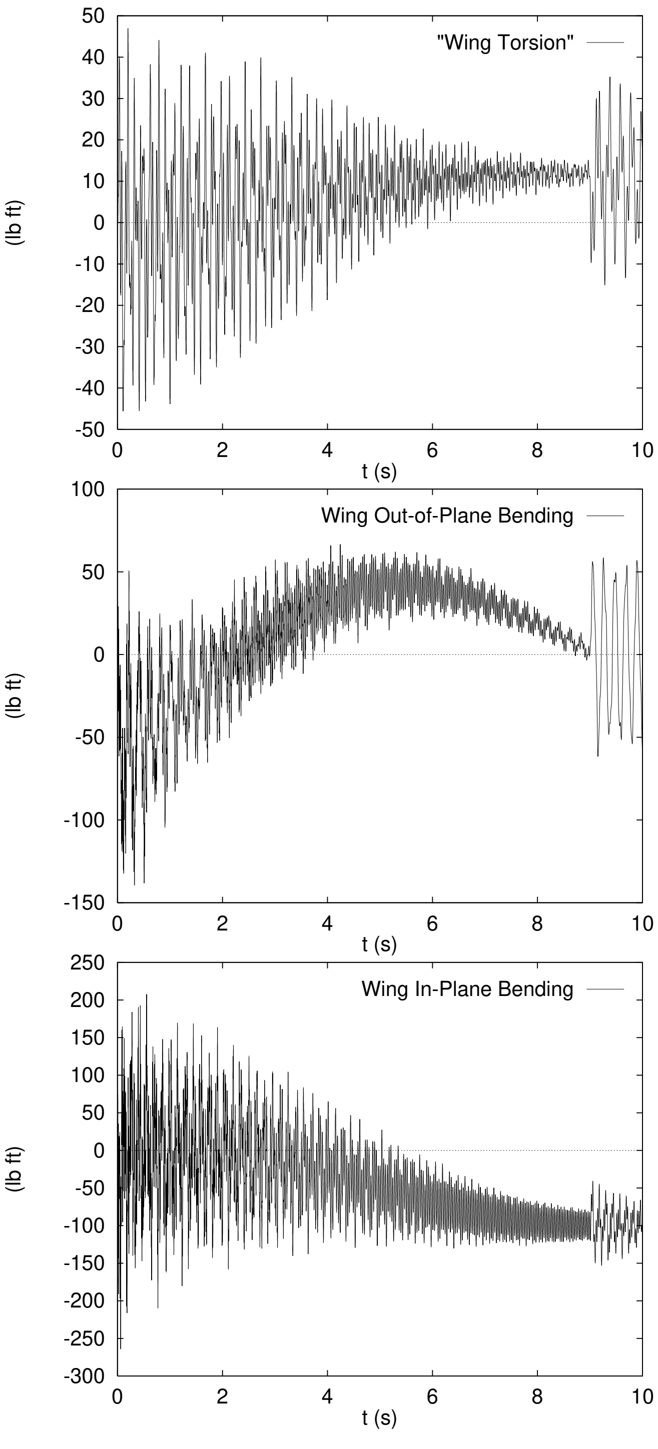

Figure 10: *Internal moments at the wing root during the conversion maneuvre, flexible blade model*

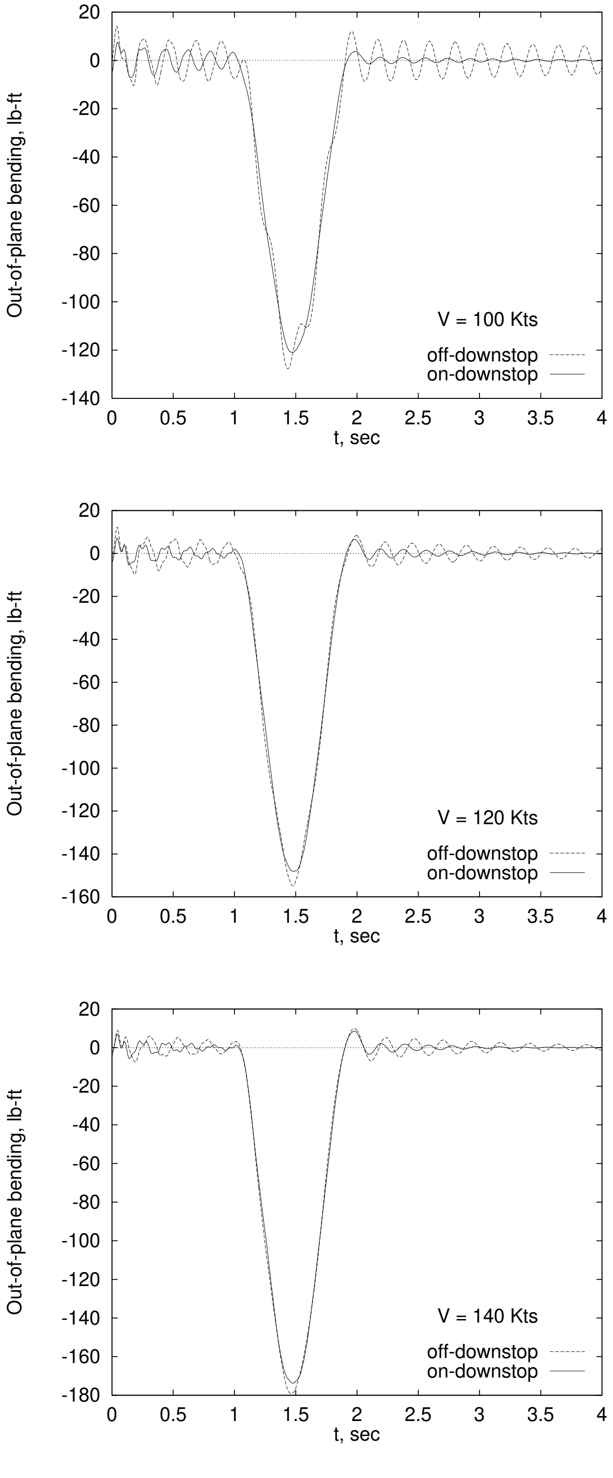

Figure 11: *Out-of-plane bending moment of the wing due to a vertical gust of 10 ft/s at airstream speeds 100–140 Kts, flexible blade model*

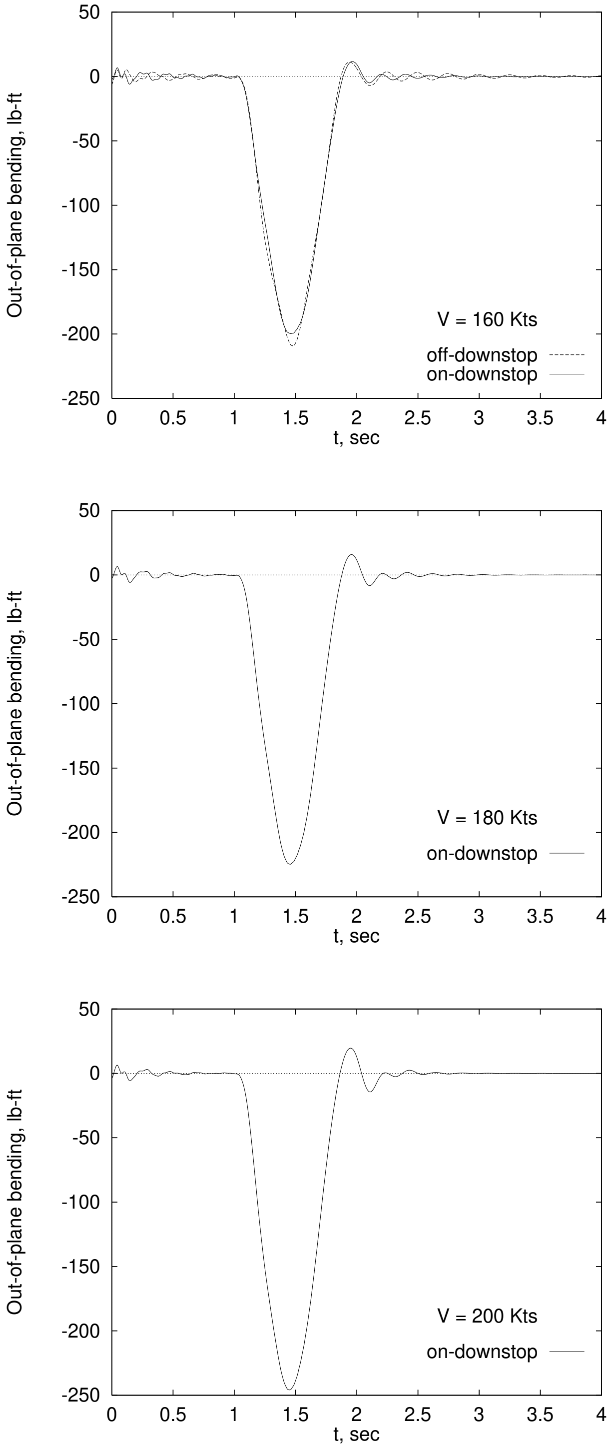

Figure 12: *Out-of-plane bending moment of the wing due to a vertical gust of 10 ft/s at airstream speeds 160–200 Kts, flexible blade model*